14TH CANADIAN MASONRY SYMPOSIUM
MONTREAL, CANADA
MAY 16TH – MAY 20TH, 2021

SEISMIC RESPONSE OF GFRP-REINFORCED MASONRY SHEAR WALLS WITH BOUNDARY ELEMENTS

Hamzeh, Layane[1]; Hassanein, Ahmed[2] and Galal, Khaled[3]

ABSTRACT

Reinforced masonry (RM) shear walls with boundary elements (BE) have been recently presented as a ductile alternative to RM rectangular shear walls. The present study addresses the applicability of reinforcing masonry shear walls with glass fibre-reinforced polymer (GFRP) bars to attain reasonable strength and drift. GFRP-RM shear walls are a corrosion-free lateral resisting system that is transparent to magnetic fields and radio frequencies and nonconductive thermally and electrically. A numerical macro-model is developed using OpenSees to simulate the in-plane response of flexure-dominated reinforced masonry shear walls with boundary elements (RMSW+BE). The model was validated against experimentally tested walls from the literature. The boundary elements were designed with C-shaped masonry blocks. A numerical study is performed on ten flexure-dominated shear walls to evaluate the influence of different design parameters on the inelastic behaviour of RMSW+BEs reinforced with GFRP bars under quasi-static fully reversed cyclic loading. The investigated parameters are transverse hoop spacing, amount of vertical reinforcement in the boundary element, and aspect ratio of the wall. The influence of the design parameters on the hysteretic response, stiffness degradation, and effective stiffness was investigated to evaluate the enhancement in the seismic performance of RM buildings with RMSW+BE.

KEYWORDS: *masonry, shear walls, GFRP, seismic response, boundary elements*

[1] Ph.D. graduate, Department of Building, Civil and Environmental Engineering, Concordia University, 1515 St. Catherine West, Montreal, QC, Canada, layan.hamze@live.com
[2] Postdoctoral fellow, Department of Building, Civil and Environmental Engineering, Concordia University, 1515 St. Catherine West, Montreal, QC, Canada, Ahmed.Hassanein@concordia.ca
[3] Professor, Department of Building, Civil and Environmental Engineering, Concordia University, 1515 St. Catherine West, Montreal, QC, Canada, khaled.galal@concordia.ca

INTRODUCTION

Reinforced masonry shear walls (RMSWs) are the primary lateral force-resisting system in reinforced masonry structures that are commonly used in low and mid-rise buildings. Rectangular RMSW typically accommodates only one layer of vertical reinforcement bars. Consequently, this single bar per cell does not allow the placement of confinement hoops at the end zones of the wall, which are subjected to high inelastic strains during an earthquake. In order to enhance the ductility and the overall seismic response of RMSW, boundary elements, BEs are used to confine the end zones. Adding BEs to RMSW can accommodate more than one layer of vertical bars, which provide a reinforcing cage that confines the end region, increases the compressive strength capacity, and delay the buckling of the vertical reinforcement. The behaviour of reinforced masonry shear walls with boundary elements (RMSW+BE) is characterized by a small compression zone, which decreases curvatures at the onset of the yield of the vertical reinforcement and increases curvatures at ultimate conditions. Boundary elements provide the required space for two layers of vertical reinforcement, which allows adding confinement hoops. This allows engineers to decrease the spacing between hoops in the boundary elements and eliminates the limitations associated with regular concrete blocks (i.e., stretchers) utilized in previous studies [1,2].

Glass fibre-reinforced polymer (GFRP) bars have been innovatively used as reinforcement in structures due to their corrosion resistance in harsh climate conditions. Mohamed et al. [3] conducted a study that involved three concrete shear walls reinforced with GFRP bars with different aspect ratios tested under combined reversed lateral and axial loading. Results indicated that shear walls that were reinforced with GFRP bars exhibited appropriate performance in resisting lateral loads associated with adequate strength and deformation capacity. Moreover, there was no strength degradation in GFRP-reinforced walls. They also achieved a higher drift ratio of 3.1% compared to 2.5% for similar walls reinforced with steel. Recent experimental studies [4] addressed the effect of the confinement level through testing six full-scale GFRP-reinforced shear walls under quasi-static cyclic loading with different confinement configurations. The obtained results demonstrate that increasing the confinement level in BEs enhanced the deformability of the walls by developing a higher level of concrete compressive strains and a better distribution of shear strains over the height of the wall. The focus of the current study is to investigate the effect of changing confinement ratio (i.e., by changing the hoop spacing), amount of vertical reinforcement ratio in BE, BE length, and aspect ratio, AR on the lateral response behaviour of GFRP-reinforced masonry shear walls with boundary elements (RMSW-BE). In this study, a nonlinear numerical model was developed and validated using OpenSees created by McKenna et al. [5] to investigate the effect of different design parameters on the lateral behaviour of RMSW-BE. Ten fully grouted RMSW-BE were modelled under simulated quasi-static cyclic loading to study the influence of design parameters on the wall load-displacement response and ductility.

NONLINEAR NUMERICAL MODELLING APPROACH

Model overview

In this study, *OpenSees* modelling software is used to create macro models of the in-plane response of RMSW-BE. The proposed model uses displacement-based (DB) beam-column elements, which assume a linear curvature distribution and a constant axial strain. A DB beam-column element with a fibre cross-section was used in order to model the shear wall components. The DB beam-column element was based on a displacement formulation that allows for distributed plasticity modelling. The nonlinear response of the element is therefore derived from the nonlinear stress-strain relationships for each fibre (masonry and reinforcement). The formulation of the fibre DB beam-column element is based on sectional analysis; therefore, it does not consider bond-slip effects and neglects the effect of shear deformations. As such, additional behavioural features were included in the model to account for these aspects.

Material models

Masonry

There are no pre-defined constitutive material models developed to simulate the response of grouted concrete masonry in most of the available numerical modelling programs such as OpenSees. Previous research studies demonstrated that the anisotropic characteristics of unreinforced masonry are substantially reduced when concrete masonry is fully grouted and well-detailed with horizontal and vertical reinforcement [6,7]. Consequently, the nonlinear cyclic response of masonry is modelled using the uniaxial concrete model (*Concrete02 material*) developed by Mander et al. [8]. The behavioural differences between concrete and fully grouted concrete masonry are accounted for by the proper definition of the material properties; this is also verified by comparing the simulated global response against the experimental results from the testing of fully grouted RM shear walls. Table 1 present the compressive strength, elasticity modulus, and ultimate strain of the masonry used in the current study.

Table 1: Material mechanical properties utilized in the numerical models

Parameter		**Value**
Grouted Masonry	Compressive strength, f'_{mo} (MPa)	17
	Elasticity modulus of masonry E_m (MPa)	14850
	Strain at peak strength, ε_{mo}	0.0015
GFRP	Elasticity modulus of GFRP bars, E_f (MPa)	50,000
	Ultimate strength of GFRP bars, f_{fu} (MPa)	1100

GFRP reinforcement

The GFRP bars are characterized by it is elastic linear response under both tension and compression loading. The contribution of GFRP bars in compression was considered by assuming the ultimate compressive strength capacity equal to 50% of the ultimate tensile strength capacity [9], while the elastic modulus of the compression curve was assumed the same as the tensile

modulus. The GFRP bars were modelled using uniaxial *Elastic material* in OpenSees using the mechanical properties shown in Table 1. The Elastic Material was combined with *MinMax material* taking into consideration the ultimate strain capacity of GFRP bars.

Transverse confinement

The FRP confined masonry was simulated using a modified version of Lam and Teng [10] model intended for FRP external wrapping. The model was modified to account for the difference in behaviour and geometry of discrete ties by Hassanein et al. [4]. This modified model accounts for the unique characteristic of continuously increasing the confining pressure during the loading history due to the linear characteristics of the FRP material. The model also accounts for the reduced strength capacity at the bent portion of the confining FRP stirrups compared to the straight portion.

Strain penetration effects

The strain penetration effect was considered in the modelling of RMSWs to avoid overestimating the wall's stiffness. If strain penetration is neglected, it will lead to underestimating the overall lateral drift of the wall. Kowalski et al. [11] found that this effect makes a relatively considerable contribution to the total lateral deformation of flexural members. Hence, in the current study, the strain penetration effect was considered using a zero-length element at the base of the wall segments. The stress-slip model proposed by Zhao and Sritharan [12] was used to consider the strain penetration effects in wall-footing intersections. A rotational spring at the base of the wall was used to model the bond-slip of the wall using (*Bond SP01 material*) available in the OpenSees platform to represent the vertical reinforcement.

Shear deformations

Most fibre elements do not account for the effect of shear deformations that occur due to lateral load, although experimental research shows that the flexure and shear displacements are coupled for most of the walls, even for walls with a relatively high aspect ratio [13]. Subsequently, it was necessary to account for shear deformations in the adopted model. Therefore, the shear deformations in the walls were aggregated using a uniaxial material model available in the OpenSees platform (*Pinching4 material*) to facilitate accurate predictions of wall displacements.

Section fibre model

In the fibre model approach utilized in this study, the cross-section is subdivided into several fibres acting in parallel. The corresponding uniaxial stress-strain relationships, as defined in the previous subsection for masonry and reinforcement, are assigned to the section fibres. The boundary elements are discretized to differentiate between the confined (regions inside the confining hoops) and the unconfined (face shell and concrete grout regions outside the confining hoops) portions of the cross-section. As such, the confining effect on the stress-strain response is only considered for the confined grout core in the boundary elements.

Element model

The choice of element length is essential when displacement-based beam-column elements are used with distributed plasticity and strain-softening material definitions [14]. In RM structural walls, the strain localization will be concentrated in the first element above the wall base. Therefore, it was highlighted by several researchers that the use of the plastic hinge length, L_p for the first element above the wall base, produces accurate and objective results [15]. However, Calabrese et al. [16] highlighted that localization and strain concentrations occur in the extreme integration point and not the extreme element. Therefore, the length of the extreme member could be twice the plastic hinge length ($2*L_p$) in the typical case of two integration sections per element. This regularization technique achieves an objective global response in cases where softening sectional behaviour is present. A schematic of the numerical model of the wall is illustrated in Fig. 1, including the configuration of nodes and elements. All walls were assumed to have perfect base fixity, and soil-structure interaction was neglected as per the NIST study [17]. It consists of an extreme member (1st element) with a length equal to twice the plastic hinge and three members with equal lengths. Several formulae are available in the literature to estimate the plastic hinge length, L_p, of shear walls [18,19]. However, none of these formulae provided accurate results for the experimental RMSW-BE considered in this paper. The formula for plastic hinge proposed by Bohl and Adebar [20], which is based on nonlinear finite element analysis results of twenty-two isolated reinforced concrete shear walls, was found to give the best estimate of L_p for the RMSW with and without boundary elements. In addition, it is one of the few formulas that account for the axial load effect on the inelastic displacement capacity of walls. Thus, it is deemed appropriate to be utilized in calculating the plastic hinge length for the proposed model.

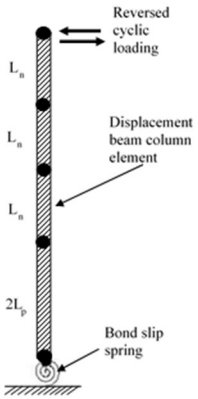

Figure 1: Schematic diagram of the element discretization used in the numerical model

VALIDATION OF THE NUMERICAL MODEL

The proposed nonlinear modelling approach, along with the calibrated material modelling parameters implemented in this study, were validated against experimental response provided in the literature. It should be noted that there were no tests found in the literature for masonry shear walls reinforced with GFRP bars. Hence the authors calibrated the numerical model with concrete

shear walls reinforced with GFRP bars since the behaviour is expected to be similar to that of RMSW, due to the similar behaviour of masonry compared to concrete and confined concrete compared to masonry core confined grout. In order to validate the modelling approach and the assumed failure criteria, one RC wall was modeled from Hassanein et al. [4]; this wall was selected as it has similar reinforcement, wall dimensions, and boundary elements detailing to the walls under study. Table 2 shows a summary of the walls' details used in numerical model validation, and Fig. 2 shows the cross-section of the modeled walls. The same loading protocol used in the experimental tests was used to compare the numerical model and experimental test results. In addition, the values of masonry and steel material model parameters were based on material tests reported in the experimental study [4]. Fig. 2 shows a comparison between the experimental and the numerical load-displacement response of the walls.

Table 2: Summary of wall details used for numerical model validation

ID.	Reference	f'_c MPa	L_w mm	H_w mm	AR	Boundary		Vertical		Horizontal		Axial stress MPa
						No. and size	ρ_{vb} %	No. and size	ρ_v %	Size @ spacing (mm)	ρ_h %	
GnoX	Hassanein et al. [4]	29.5	1500	3500	2.33	8 #3	1.73	18 #3	0.55	#4 @ 80	1.6	4.43

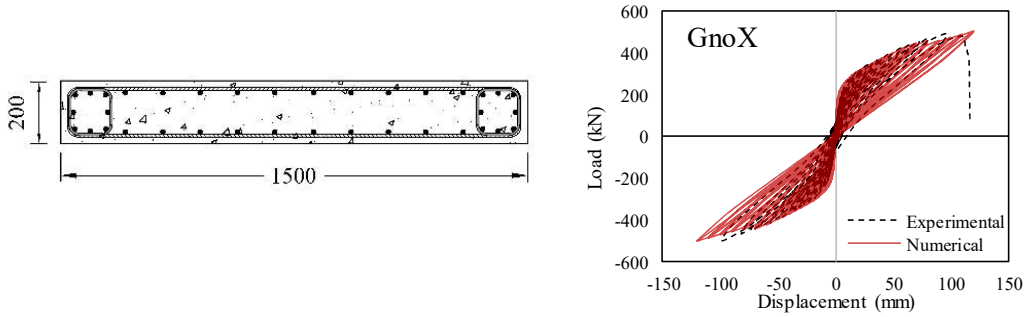

Figure 2: Cross-section details of GnoX (Hassanein et al. [4]), and Experimental and numerical load-displacement response.

It can be seen that the numerical model is in good agreement with the hysteretic responses of the experimental test results. The numerical model is capable of simulating the initial stiffness, yield, and ultimate strengths, displacements, loading, and unloading of the post-peak branches. The model was able to compute the RMSW+BEs lateral capacity with high accuracy. Also, the key parameters of the behaviour were captured by the numerical model, with a maximum error of 7.0%. Overall.

PARAMETRIC STUDY

Ten fully grouted RMSW-BE were modelled using the DB beam-column elements nonlinear numerical modelling approach described earlier utilizing OpenSees. The numerical model was used to investigate the effect of different design parameters on the load-displacement response of RMSW-BE under quasi-static cyclic loading. These parameters include the amount of vertical

reinforcement ratio in BE, BE size, spacing of transverse reinforcement in BE, and aspect ratio of the wall. The following sections provide details about the wall selection criteria, wall details, and wall design considered in this study. All the walls had the same length, and this was an important criterion to be able to determine the effect of the proposed wall end configuration on the overall response when walls with square-shaped BE were replaced with rectangular-shaped BE. In addition, the same vertical reinforcement ratio was utilized in both wall configurations (i.e., walls with square-shaped and rectangular-shaped BE) in order to allow for comparison between the walls in terms of the overall wall response. Furthermore, all the walls considered in the current study have a shear span-to-depth ratio greater than or equal to 1.5 and designed to fail in a flexural mode.

Wall details and design

Table 3 shows a summary of the wall details (i.e., dimensions and reinforcement) used in the parametric study. Boundary element length (L_{BE}) and width (B_{BE}) have been selected to be 390 mm and 390 mm for square-shaped BE, and 780 mm and 390 mm for rectangular-shaped BE, respectively. Besides, a web length of 3510 mm, and a web thickness of 190 mm were utilized for all walls. Hence, the total length of all the walls, L_w was 5070 mm. The GFRP- reinforced walls were detailed with #6 (20M) vertical GFRP bars (A_v=284 mm^2), and #3 (10M) horizontal GFRP bars (A_h=71 mm^2). Fig. 3 shows the cross-sections for RMSW+BEs with different BE detailing configurations.

Table 3: Summary of wall details used in the parametric study

#	Wall ID.	L_w m	H_w m	*AR*	Boundary element					Web		Axial stress MPa
					L_{BE} mm	B_{BE} mm	Vertical bars No. and size	Hoops size @spacing	*Reinf. ratio* ρ_{vb} %	Vertical bars No. and size	Horizontal bars size @ spacing	
1	S12G4-60	5.1	12	2.4	390	390	4-20M	10M@60	0.75	6-20M	20M@200	0.60
2	S15G4-60	5.1	15	3.0	390	390	4-20M	10M@60	0.75	6-20M	20M@200	0.75
3	S18G4-60	5.1	18	3.5	390	390	4-20M	10M@60	0.75	6-20M	20M@200	0.90
4	S12G8-60	5.1	12	2.4	390	390	8-20M	10M@60	1.50	6-20M	20M@200	0.60
5	S12G4-120	5.1	12	2.4	390	390	4-20M	10M@120	0.75	6-20M	20M@200	0.60
6	S12G8-120	5.1	12	2.4	390	390	8-20M	10M@120	1.50	6-20M	20M@200	0.60
7	R12G4-60	5.1	12	2.4	780	390	8-20M	10M@60	0.75	6-20M	20M@200	0.60
8	R12G8-60	5.1	12	2.4	780	390	16-20M	10M@60	1.50	6-20M	20M@200	0.60
9	R12G4-120	5.1	12	2.4	780	390	8-20M	10M@120	0.75	6-20M	20M@200	0.60
10	R12G8-120	5.1	12	2.4	780	390	16-20M	10M@120	1.50	6-20M	20M@200	0.60

Two different spacings between transverse reinforcement were implemented in the boundary elements 60 mm, and 120 mm. In addition, two vertical reinforcement ratios in the boundary element were investigated: i.e. four 20M bars (ρv_{BE} = 0.78%), and eight 20M bars (ρv_{BE}=1.58 %). Furthermore, three AR were considered: 4 stories (AR=2.4), 5 stories (AR=3), 6 stories (AR=3.5). The axial stress was taken as 0.15 MPa per story for all walls resulting in 0.60, 0.75, and 0.90 MPa for 4, 5, and 6 stories walls, respectively. The RMSW-BEs considered in the parametric study were designed to be controlled by flexural behaviour according to CSA S304 [21] standard with a safe

margin for the shear capacity to avoid undesirable shear failure. Therefore, the walls had shear capacities much larger than the shear forces corresponding to the predicted flexural strength.

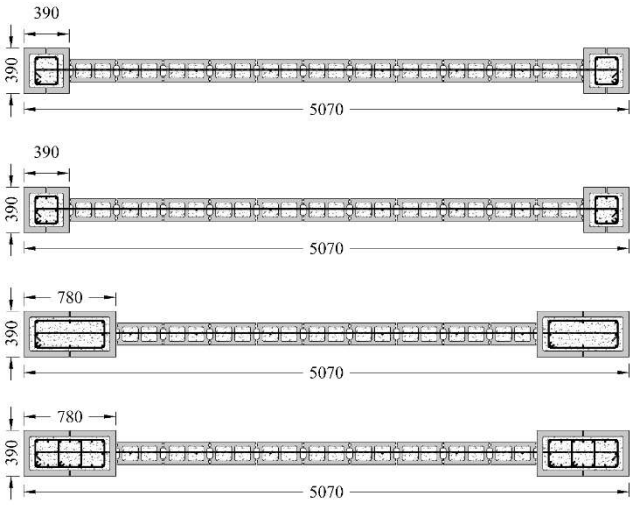

Figure 3: Cross-sections for RMSW-BE: (a) Square BE with 4 bars; (b) Square BE with 8 bars; (c) Rectangular BE with 8 bars; (d) Rectangular BE with 16 bars

RESULTS AND DISCUSSION

Lateral load-displacement response

For all the walls, the axial loads were held constant, and reversed cyclic horizontal displacements at increasing increments of the yield displacement were applied at the top of the wall. The envelope of the load-displacement hysteretic curves for each wall was generated. Fig. 4 shows the typical hysteretic response and envelope for wall S12G4-60.

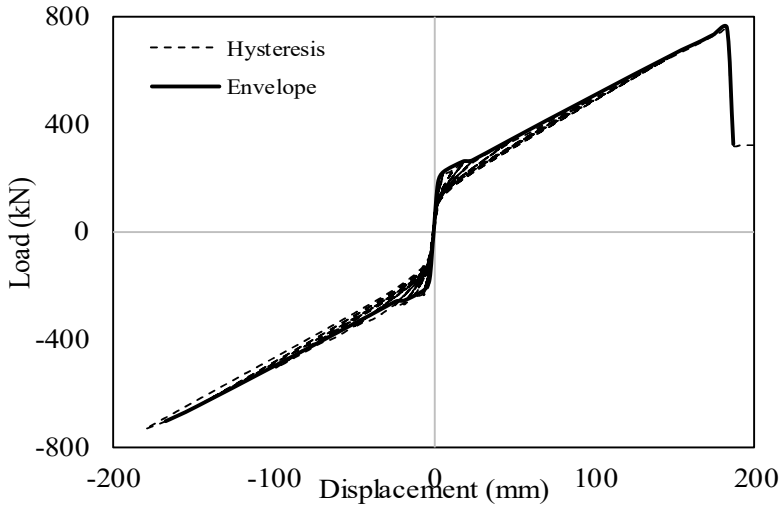

Figure 4: Typical load-displacement hysteresis and envelope wall S12G4-60

The hysteretic behaviour of the GFRP-reinforced walls showed pinched hysteric loops with symmetric lateral load-displacement relationship for loading in both the +ve and –ve direction until failure occurred at one end. The failure developed in GFRP-reinforced walls when the strain in the longitudinal bars at the extreme fibre reached it is ultimate capacity. The cycles in GFRP-reinforced walls had a minimal residual force when the returns to its original position, similar to the walls tested by Hassanein et al. [22]. The GFRP-reinforced walls reached the ultimate strength and no strength degradation up to the peak point. The unloading and reloading curves showed linearity due to the GFRP elastic behaviour. The load and displacement at each stage are presented in Table 4.

Ductility related force modification factor

Having a reliable estimation of the R_d factor by defining its relation to the wall displacement ductility is essential for efficient seismic design. According to Newmark and Hall [23], the R_d factor can be defined based on either equal energy or equal displacement principle depending on the period of vibration of the structure. In order to estimate R_d for GFRP-reinforced walls, the load-displacement response was idealized with the linearly elastic-perfectly plastic curve using the equivalent energy elastic-plastic (EEEP) method. According to current design codes, the elastic-plastic transition point represents the design capacity equal to or exceeding the required factored code-specified seismic force P_1, which is the maximum load, (Fig. 5). P_2 is the seismic design force due to an earthquake of intensity specified in the given seismic map area but corresponding to full elastic structural response. The value of $P2$ was obtained using an equal-energy principle (Fig. 5). R_d is defined as the ratio between the lateral elastic load, P_2, and the idealized wall capacity, P_1. As listed in Table 4, the GFRP-reinforced masonry shear walls had R_d values ranging from 1.8 to 4.6. Based on the estimated values, the lower bound value of R_d =1.5 is recommended for the studied walls.

Table 4: Numerical modelling results and Rd values

Wall ID.	Q_u (kN)	Δ_u (mm)	P_1 (kN)	P_2 (kN)	$R_d = P_2/P_1$
S12G4-60	754.8	182.6	570	1321	2.3
S15G4-60	586.9	262.5	395	1375	3.5
S18G4-60	492.9	342.3	305	1406	4.6
S12G8-60	1078.6	186.9	825	1677	2.0
S12G4-120	757.5	183.0	555	1235	2.2
S12G8-120	1039.8	181.5	720	1538	2.1
R12G4-60	1014.4	190.7	773	1568	2.0
R12G8-60	1617.5	208.2	1210	2314	1.9
R12G4-120	1026.5	188.2	780	1604	2.1
R12G8-120	1562.4	189.9	1325	2369	1.8

Effect of vertical reinforcement ratio

The amount of vertical reinforcement had a significant effect on the load-displacement relationship. As ρ_{vBE} increased, there was an increase in ultimate strength of the wall increased. For walls with square-shaped BE, the lateral load increased by 43% and 37% for S_{hoop}= 60 mm and 120 mm, respectively. A similar trend was also observed for walls with rectangular shaped BE where the lateral load increased by 60% and 52% for S_{hoop}= 60 mm and 120mm, respectively.

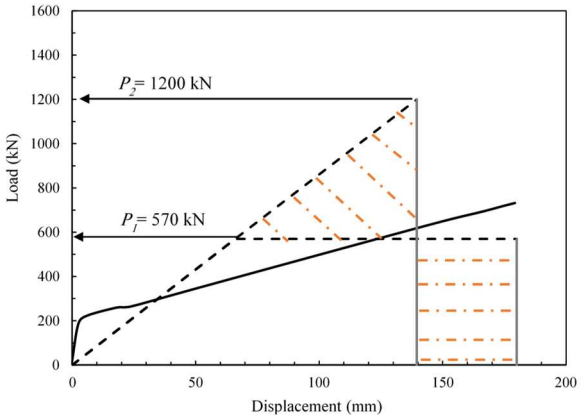

Figure 5: Determination of the equivalent linear elastic response for wall S12G4-60

Size of boundary element

In this section, the effect of changing the size of BE on the load-displacement behaviour is evaluated. Based on the results from Table 4, the maximum lateral load increased for walls with AR = 2.4, 3.0, and 3.5 by changing the length of BE from 390 mm to 780 mm. Results show that increasing the size of BE resulted in a slight improvement in the ultimate displacement of GFRP-reinforced walls. It was observed that there is an increase in the lateral load of 50% and 35% for walls with rectangular shaped BE for walls, and having ρv_{BE} =1.58% and 0.79%, respectively.

Aspect ratio

The relationship between the wall's aspect ratio and load-displacement behaviour is evaluated for three different aspect ratios. Results show that increasing AR from 2.4 to 3.5, the peak strength of the wall decreased. The three walls (S12G4-60, S15G4-60, S18G4-60) were able to achieve their

flexural capacity with no strength degradation. Wall S18G4-60 with AR=3.5 had lower Q_u= 492.9 kN compared to wall S12G4-60 with AR=2.4 and Q_u=754.8 kN. However, wall S18G4-60 achieved higher deformations compared to walls S15G4-60 and S18G4-60, as shown in Table 4. For walls with square-shaped BE, and low confinement (i.e. S_{hoop} = 60 mm), as the AR increased from 2.4 to 3.5, the ultimate displacement decreased by 6% for ρ_{vBE} = 0.79% and decreased by 5% for ρv_{BE}= 1.58%. In addition, for walls with square-shaped BE with high confinement (i.e. S_{hoop} = 120 mm), the ultimate displacement decreased by 19% for walls with ρ_{vBE} = 0.79% and decreased by 35% for walls with ρ_{vBE} = 1.58%. Walls with rectangular-shaped BE, and low confinement (i.e. S_{hoop} = 60 mm), the ultimate displacement decreased by 24% for walls with ρ_{vBE} = 0.79%, and by 23% for ρ_{vBE} = 1.58%, as AR increased. Similarly, as AR increased for walls with rectangular-shaped BE, high confinement (i.e., S_{hoop} = 120 mm), the ultimate displacement decreased by 37% for walls with ρ_{vBE} = 0.79%, and by 21.9% for walls with ρ_{vBE} =1.58%.

CONCLUSIONS

The GFRP-reinforced walls reached the ultimate design strength through a typical linear envelope curve with no strength degradation. The elasticity of the GFRP reinforcement and the absence of yielding phenomena caused an increase in strength up to failure. GFRP-reinforced shear walls behave elastically up to near failure with much higher strength capacity compared to steel. The hysteretic response of the GFRP-walls is pinched with minimal residual strength and much lower energy dissipation capacity. Therefore, GFRP-walls can be used in low to mid seismic zones where the seismic demand can be resisted by the elastic response limited to the permissible limits of GFRP bars. The value of the seismic force modification factor, R_d, for GFRP-reinforced walls was evaluated based on the idealized curve and found to range from 1.8 to 4.6. A conservative value of R_d=1.5 is recommended.

ACKNOWLEDGMENTS

The authors acknowledge the support from the Natural Science and Engineering Research Council of Canada (NSERC), the Canadian Concrete Masonry Producers Association (CCMPA), Canada Masonry Design Centre (CMDC), and L'Association des Entrepreneurs en Maçonnerie du Québec (AEMQ).

REFERENCES

[1] Shedid, M., El-Dakhakhni, W., and Drysdale, R. (2010). “Alternative Strategies to Enhance the Seismic Performance of Reinforced Concrete-Block Shear Wall Systems.” Journal of Structural Engineering, 136(6), 676-689.

[2] Banting, B., and El-Dakhakhni, W. (2012). “Force- and Displacement-Based Seismic Performance Parameters for Reinforced Masonry Structural Walls with Boundary Elements.” Journal of Structural Eng., 138(12), 1477-1491.

[3] Mohammed, N., Farghaly, A. S., Benmokrane, B., and Neale K.W. (2014). “Experimental investigation of concrete shear walls reinforced with glass fiber-reinforced bars under lateral cyclic loading. ” Journal of Composites for Construction, ASCE, 18(3), 04014001.

[4] Hassanein, A., Mohamed, N., Farghaly, A., and Benmokrane, B. (2019b) "Modeling of Hysteretic Response for GFRP-Reinforced Concrete Walls" ACI Structural Journal, 116-S122.
[5] McKenna, F., Fenves, G. L., Scott, M. H., and Jeremic, B., (2013). "Open System for Earthquake Engineering Simulation (OpenSees)." Pacific Earthquake Engineering Research Center, University of California, Berkeley.
[6] Banting, B., and El-Dakhakhni, W. (2014). Seismic performance quantification of reinforced masonry structural walls with boundary elements. Journal of Structural Engineering, 140(5), 1–15.
[7] Drysdale, R. G., and Khattab, M. M. (1995). In-plane behavior of grouted concrete masonry under biaxial tension-compression. ACI Structural Journal, 92(6), 653–664.
[8] Mander, J. B., Priestley, M.J.N., and Park, R. (1988). "Theoretical stress-strain model for confined concrete." Journal of Structural Engineering, 114:8(1804), 1804-1826.
[9] De Luca, A., Matta, F., and Nanni, A. (2009). "Behavior of Full-Scale Concrete Columns Internally Reinforced with Glass FRP Bars under Pure Axial Load." COMPOSITES & POLYCON , American Composites Manufacturers Association, January 15-17, Tampa, FL USA, 1-10.
[10] Lam, L., and Teng, J. (2003). "Design-Oriented Stress-Strain Model for FRP-Confined Concrete in Rectangular Columns." Journal of Reinforced Plastics and Composites, 22(3), 1149-1186.
[11] Kowalsky, M. J., Priestley, M. J. N., and Seible, F. (1999). "Shear and flexure behavior of lightweight concrete bridge columns in seismic regions." ACI Struct. J., 96(1), 136–148.
[12] Zhao, J., and Sritharan, S. (2007). "Modeling of strain penetration effects in fiber-based analysis of reinforced concrete structures." ACI Struct. J., 104 (2), 133–141.
[13] Massone, L. M., and Wallace, J. W. (2004). "Load-deformation responses of slender reinforced concrete walls." ACI Structural Journal, 101:1, 103-113.
[14] Lowes, L., Lehman, D., Kuchma, D., Mock, A., and Behrouzi, A. (2013). "Large scale tests of C-shaped reinforced concrete walls." ⟨https://nees .org/warehouse/project/104⟩.
[15] Ezzeldin, M., Wiebe, L., Shedid, M., and El-Dakhakhni, W. (2014). "Numerical modelling of reinforced concrete block structural walls under seismic loading." 9th Int. masonry conf., Guimarães, Portugal.
[16] Calabrese, A., Almeida, J., and Pinho, R. (2010). "Numerical Issues in Distributed Inelasticity Modeling of RC Frame Elements for Seismic Analysis." J of Earthquake Eng. 14(sup1), 38-68.
[17] NIST. (2010). "Evaluation of the FEMA P695 methodology for quantification of building seismic performance factors." NIST GCR 10-917-8, Gaithersburg, MD.
[18] Park, R., and Paulay, T. (1975). "Reinforced concrete structures." John Wiley and Sons, New York.
[19] Paulay, T., and Priestley, M. J. N. (1992). "Seismic design of reinforced concrete and masonry buildings" Wiley, New York.
[20] Bohl, A., and Adebar, P. (2011). "Plastic Hinge Lengths in High-Rise Concrete Shear Walls." ACI Structural Journal, 108(2), 148-157.
[21] CSA (Canadian Standards Association). (2014). "Design of masonry structures." CSA S304.14, Mississauga, Canada.
[22] Hassanein, A., Mohamed, N., Farghaly A. S., and Benmokrane, B., (2020), "Effect of boundary element confinement configuration on the performance of GFRP-Reinforced concrete shear walls.", Engineering Structures, 225, 111262.
[23] Newmark N.M., and Hall W.J. (1982). "Earthquake spectra and design." Earthquake Engineering Research Institute, Berkeley, C.A.